

## DISCOVERY OF OUTLYING, HIGH-VELOCITY OXYGEN-RICH EJECTA IN CASSIOPEIA A<sup>1</sup>

ROBERT A. FESEN<sup>2</sup>, MOLLY C. HAMMELL<sup>2</sup>, JON MORSE<sup>3</sup>, ROGER A. CHEVALIER<sup>4</sup>, KAZIMIERZ J. BORKOWSKI<sup>5</sup>, MICHAEL A. DOPITA<sup>6</sup>, CHRISTOPHER L. GERARDY<sup>7</sup>, STEPHEN S. LAWRENCE<sup>8</sup>, JOHN C. RAYMOND<sup>9</sup>, & SIDNEY VAN DEN BERGH<sup>10</sup>

(Received 2005 July 30)  
*Submitted to the Astrophysical Journal*

### ABSTRACT

Analysis of broadband *HST* ACS and WFPC2 images of the young Galactic supernova remnant Cassiopeia A reveals a far larger population of outlying, high-velocity knots of ejecta with a broader range of chemical properties than previously suspected. ACS filter flux ratios along with follow-up, ground-based spectra are used to investigate some of the kinematic and chemical properties of these outermost ejecta. In this paper, we concentrate on a  $\simeq 1.5$  sq arcmin region located along the eastern limb of the remnant where numerous outer emission knots are optically visible due to an interaction with a local circumstellar cloud, thereby providing a more complete and unbiased look at the remnant's fastest debris fragments. From a study of this region, we identify three main classes of outer ejecta: 1) Knots dominated by [N II]  $\lambda\lambda 6548, 6583$  emission; 2) Knots dominated by oxygen emission lines especially [O II]  $\lambda\lambda 7319, 7330$ ; and 3) Knots with emission line strengths similar to the [S II] strong FMK ejecta commonly seen in the main emission shell. We identified a total of 69 [N II], 40 [O II], and 120 [S II] knots in the small eastern limb region studied. Mean transverse velocities derived from observed proper motion for 63 N-rich, 37 O-rich, and 117 FMK-like knots identified in this region were found to be 8100, 7900, and 7600 km s<sup>-1</sup>, respectively.

The discovery of a significant population of O-rich ejecta situated in between the suspected N-rich outer photospheric layer and S-rich FMK-like ejecta suggests that the Cas A progenitor's chemical layers were not completely disrupted by the supernova explosion outside of the remnant's NE and SW high velocity 'jet' regions. In addition, we find the majority of O-rich outer ejecta at projected locations out beyond ( $v = 6500 - 9000$  km s<sup>-1</sup>) the remnant's fastest moving Fe-rich X-ray emission material (6000 km s<sup>-1</sup>) seen in *Chandra* and *XMM* data along the eastern limb. This suggests that penetration of Fe-rich material up through the S and Si-rich mantle did not extend past the progenitor's N or O-rich outer layers for at least this section of the remnant.

*Subject headings:* ISM: individual (Cassiopeia A) - ISM: kinematics and dynamics - ISM: abundances - supernova remnants

### 1. INTRODUCTION

With an estimated explosion date no earlier than  $1671 \pm 1$  (Thorstensen, Fesen, & van den Bergh 2001) and an estimated distance of  $3.4^{+0.3}_{-0.1}$  kpc (Reed et al. 1995), the bright radio source Cassiopeia A (Cas A) is currently the youngest known Galactic remnant of a

core-collapse supernova (SN). The remnant consists of an optical, infrared, and X-ray bright 4' diameter ( $\simeq 4$  pc) emission ring of reverse shock heated SN debris rich in O, Si, S, Ar, Ca and Fe (Chevalier & Kirshner 1978, 1979; Douvion et al. 1999; Hughes et al. 2000; Willingale et al. 2002; Hwang & Laming 2003). Optically, the remnant's SN debris are seen as condensations and filaments known collectively as Fast-Moving Knots (FMKs), with expansion velocities between 4000 – 6000 km s<sup>-1</sup> (Minkowski 1968; van den Bergh 1971; Lawrence et al. 1995; Reed et al. 1995).

Estimates for the initial main sequence mass of the Cas A progenitor are between 10 and 30  $M_{\odot}$  (Fabian et al. 1980; Vink et al. 1998; Willingale et al. 2003; Laming & Hwang 2003; Vink 2004). A Wolf-Rayet star progenitor has often been proposed (Langer & El Eid 1986; Fesen, Becker, & Blair 1987; Fesen & Becker 1991; García-Segura, Langer, & Mac Low 1996) and a mass-loss, ring nebula around such a progenitor is consistent with the presence of slow-moving clumps ('QSFs',  $v = 0 - 400$  km s<sup>-1</sup>) of N and He-rich, pre-SN circumstellar mass loss material (Peimbert & van den Bergh 1971; Kamper & van den Bergh 1976; Kirshner & Chevalier 1977; Chevalier & Kirshner 1978).

Along the outer periphery of the remnant's main ejecta shell, numerous small knots of ejecta have been de-

<sup>1</sup> Based on observations with the NASA/ESA Hubble Space Telescope, obtained at the Space Telescope Science Institute, which is operated by the Association of Universities for Research in Astronomy, Inc. under NASA contract No. NAS5-26555.

<sup>2</sup> 6127 Wilder Lab, Department of Physics & Astronomy, Dartmouth College, Hanover, NH 03755

<sup>3</sup> Department of Physics and Astronomy, Arizona State University, Box 871504, Tempe, AZ 85287

<sup>4</sup> Department of Astronomy, University of Virginia, P.O. Box 3818, Charlottesville, VA 22903

<sup>5</sup> Department of Physics, North Carolina State University, Raleigh, NC 27695

<sup>6</sup> Research School of Astronomy and Astrophysics, The Australian National University, Cotter Road, Weston Creek, ACT 2611 Australia

<sup>7</sup> Astrophysics Group, Imperial College London, Blackett Laboratory, Prince Consort Road, London SW7 2BZ

<sup>8</sup> Department of Physics and Astronomy, Hofstra University, Hempstead, NY 11549

<sup>9</sup> Harvard-Smithsonian Center for Astrophysics, 60 Garden Street, Cambridge, MA 02138

<sup>10</sup> Dominion Astrophysical Observatory, Herzberg Institute of Astrophysics, NRC of Canada, 5071 West Saanich Road, Victoria, BC V9E 2E7, Canada

tected at projected positions near or beyond the forward shock front (see Fesen 2001 and references therein). The brightest and best known group of such high-velocity outer ejecta lies in the northeastern ‘jet’, which consists of three or four streams of ejecta knots extending out  $\sim 2'$  from the remnant’s northeast rim. Over a hundred jet knots have been identified from ground-based images and these knots exhibit much higher proper motion derived transverse velocities ( $7000 - 14000 \text{ km s}^{-1}$ ) than the  $\sim 6000 \text{ km s}^{-1}$  FMKs seen in the main shell (van den Bergh & Dodd 1970; Fesen & Gunderson 1996). Optical imaging and spectra of FMKs in the jet show strong  $[\text{S II}] \lambda\lambda 6716, 6731$  but relatively weak or absent  $[\text{O III}] \lambda\lambda 4959, 5007$  emission. A few much fainter outer FMKs have been recently found in an apparent southwest ‘counterjet’ spatially coincident with faint extended X-ray emission (Fesen 2001; Hwang et al. 2004).

In addition to these outlying NE and SW jet FMKs, some 50 faint outlying knots with strong  $[\text{N II}] \lambda\lambda 6548, 6583$  emission but weak or absent  $\text{H}\alpha$ ,  $[\text{S II}] \lambda\lambda 6716, 6731$  and  $[\text{O II}] \lambda\lambda 7319, 7330$  line emissions have been detected around much of the remnant’s periphery (Fesen, Becker, & Blair 1987; Fesen 2001). Radial velocity measurements combined with estimated transverse velocities based on proper motion or knot displacement from the remnant’s center of expansion indicate these strong  $[\text{N II}]$  emission knots have space velocities of  $8000 - 12000 \text{ km s}^{-1}$  (Fesen 2001). These apparently N-rich knots appear to represent fragments of the progenitor’s outer layers and are consistent with the suggestion of a WN Wolf-Rayet progenitor which experienced substantial pre-SN mass-loss (the N-rich QSFs) before exploding as a Type Ib/c or Type II supernova.

In this paper, we report results from a new and much deeper survey of outer ejecta fragments in the Cas A SNR. The survey reveals a far larger population of high-velocity knots of ejecta and a broader range of chemical properties than previously suspected. A complete catalog of outer ejecta knots is beyond the scope of the present work and will be addressed in a separate paper (Hammell & Fesen 2006). Here we concentrate on the remnant’s outer ejecta rich eastern limb region and use this area to help define some of the kinematic and chemical properties of the remnant’s fastest moving ejecta. The observations are described in §2, with the results and conclusions given in §3 and §4, respectively.

## 2. OBSERVATIONS

### 2.1. Imaging

As part of an imaging survey of the ejecta in the Cas A SNR, we obtained high resolution images of the remnant between January 2000 and December 2004 using two different cameras on board the *Hubble Space Telescope* (*HST*).

Multiband images taken at six pointings covering the entire remnant, including all previously known outlying ejecta knots, were obtained on 2004 March 4–6 and 2004 December 4–5 using the Wide Field Channel (WFC) of the Advanced Camera for Surveys (ACS; Ford et al. 1998; Pavlovsky et al. 2004) on board *HST*. The ACS/WFC consists of two  $2048 \times 4096$  CCDs providing a field of view  $202'' \times 202''$  with an average pixel size of  $0''.05$ . Four 2-point line dithered images were taken in each of the four ACS/WFC Sloan Digital Sky Survey

(SDSS) filters, namely F450W, F625W, F775W, and F850LP (i.e., SDSS g, r, i, and z), at each target position to permit cosmic ray removal, coverage of the  $2''.5$  interchip gap, and to minimize saturation effects of bright stars in the target fields.

Total integration times in the F450W, F625W, F775W, and F850LP filters were 2000 s, 2400 s, 2000 s, and 2000 s respectively. Standard ACS pipeline IRAF/STSDAS<sup>11</sup> data reduction was done including debiasing, flat-fielding, geometric distortion corrections, photometric calibrations, and cosmic ray and hot pixel removal. The STSDAS *drizzle* task was used to combine exposures in each filter.

Detected counts in each of the drizzled filter images were converted to flux units by summing the signal in  $5 \times 5$  pixel windows, subtracting a local mean background and then multiplying by the mean flux density per unit wavelength generating 1 count  $\text{s}^{-1}$  (i.e., the ‘PHOTFLAM’ factor) times the filter effective bandwidth (EBW). For the F625W, F775W, and F850LP filters, the PHOTFLAM values used in units of  $10^{-19} \text{ erg cm}^{-2} \text{ s}^{-1} \text{ \AA}^{-1}$  and the EBW values used were 1.195, 1.007, 1.507, and  $415.5 \text{ \AA}$ ,  $434.6 \text{ \AA}$ , and  $539.4 \text{ \AA}$ , respectively (Sirianni et al. 2005).

Due to significant reddening toward Cas A ( $A_V = 4.5 - 8$  mag; Hurford & Fesen 1996; Reynoso & Goss 2002),  $[\text{O III}] \lambda\lambda 4959, 5007$  line emission was too weak to be detected for most outlying knots. We have, therefore, not included F450W images in our analysis. Table 1 lists the primary emission lines detected by the three other filters, the total system throughput of the telescope + ACS/WFC camera + filter, and the resulting relative line flux of a typical main shell Cas A FMK ejecta knot.

Previous *HST* images of the remnant taken on 2000 January 23 and 2002 January 16 using the Wide Field Planetary Camera 2 (WFPC2) were also analyzed, primarily to measure knot proper motions. While these WFPC2 images mainly targeted Cas A’s bright main shell (Fesen et al. 2001; Morse et al. 2004), they also included  $4 \times 500$  s F675W filter exposures of portions of the remnant’s outer eastern limb. The WFPC2 images have an image scale of  $0''.1 \text{ pixel}^{-1}$  which under-sampled *HST*’s  $0''.046$  angular resolution. The F675W filter (bandpass:  $6000 - 7600 \text{ \AA}$ ) was sensitive to line emissions of  $[\text{O I}] \lambda\lambda 6300, 6364$ ,  $[\text{N II}] \lambda\lambda 6548, 6583$ ,  $[\text{S II}] \lambda\lambda 6716, 6731$ ,  $[\text{Ar III}] \lambda 7136$ , and  $[\text{O II}] \lambda\lambda 7319, 7330$ . Further descriptions of these data and their reduction can be found in Fesen et al. (2001) and Morse et al. (2004).

### 2.2. Spectroscopy

Follow-up, low-dispersion optical spectra of a few outlying emission knots were obtained on three nights in September 2004 using the MDM<sup>12</sup> 2.4 m telescope and the Modular Spectrograph with a  $600 \text{ lines mm}^{-1}$   $6000 \text{ \AA}$  blaze grating and a  $1''.5 \times 4.0'$  slit. Typically, we obtained two 1000 s, 1500 s, or 2000 s exposures for each

<sup>11</sup> IRAF is distributed by the National Optical Astronomy Observatories, which is operated by the Association of Universities for Research in Astronomy, Inc. (AURA) under cooperative agreement with the National Science Foundation. The Space Telescope Science Data Analysis System (STSDAS) is distributed by the Space Telescope Science Institute.

<sup>12</sup> Formerly known as the Michigan–Dartmouth–MIT Observatory.

emission knot yielding a spectrum with an effective coverage of  $6000 - 8000 \text{ \AA}$  and a spectral resolution of  $\simeq 2 \text{ \AA}$ . Standard IRAF data reduction software was used with wavelengths calibrated with Hg, Ne, and Xe lamps and (Massey & Gronwald 1990) standard stars. Although all three nights were photometric, seeing was  $1''.0 - 1''.5$  leading to considerable slit light losses at times due to variable seeing conditions and guiding errors.

These data supplemented previous low-dispersion spectra of ground-based detected outlying emission knots obtained in October 1996 using the MDM 2.4 m telescope with the Mark III Spectrograph and a  $1024 \times 1024$  Tektronix CCD detector (Fesen 2001). A  $1''.2 \times 4.5'$  slit and a  $300 \text{ lines mm}^{-1}$  5400  $\text{\AA}$  blaze grism were used to obtain sets of two or three  $1000 - 1200$  s exposures spanning the spectral region  $4500 - 7400 \text{ \AA}$  with a spectral resolution of  $\simeq 8 \text{ \AA}$ . In both these and the September 2004 observations, aperture slits were oriented North-South.

### 3. RESULTS

A comparison of the 2000 and 2002 WFPC2 + F675W filter images of a small portion of the remnant's eastern-most limb revealed about 100 high proper motion ejecta knots. Most of these knots went undetected in earlier ground-based imaging surveys which had concentrated on detecting strong [N II]  $\lambda\lambda 6548, 6583$  emission knots (Fesen 2001).

Figure 1 shows the dramatic increase in the number of detected outlying ejecta knots using broadband *HST* images compared to narrowband ground-based images. The upper left-hand panel of the figure shows a  $\simeq 75'' \times 85''$  portion of the remnant's eastern limb as seen in a 2.4 m MDM image taken using a 6568  $\text{\AA}$  filter (FWHM = 90  $\text{\AA}$ ) sensitive to ejecta knots with strong [N II] emission within a limited radial velocity range ( $\pm 2500 \text{ km s}^{-1}$ ). Only a few outer knots were detected in this image (Fesen 2001). The same region imaged in January 2002 using the WFPC2 + F675W filter is shown in the lower left-hand panel of Figure 1. In contrast to the small handful of knots detected from the ground, over 100 small clumps of ejecta can be seen in the WFPC2 image with knot diameters near the image resolution ( $0''.1 \text{ pixel}^{-1}$ ). Outlying knots visible on the WFPC2 image and confirmed by the detection of proper motions  $\geq 0''.75$  between the 2000 and 2002 WFPC2 images, corresponding to  $V_{\text{trans}} \geq 6000 \text{ km s}^{-1}$  for  $d = 3.4 \text{ kpc}$ , are marked with circles on the 2002 WFPC2 image shown in the upper right-hand panel.

The location of these outlying optical ejecta knots with respect to the remnant's outermost X-ray emission, i.e., associated with the forward shock (Gotthelf et al. 2001), can be seen by comparing the knots' positions with the extent of the remnant's X-ray emission shown in the lower right-hand panel image of Figure 1. This image shows a section of the 1 Msec Chandra ACIS image (epoch 2004.3; Hwang et al. 2004) covering the same eastern region as the other panels in the figure. Nearly all the outlying optical knots seen here lie (in projection) beyond the remnant's bright main emission shell and either close to or eastward (i.e., outside) of the remnant's  $\simeq 6000 \text{ km s}^{-1}$  forward shock front as determined by the remnant's easternmost X-ray emission (Delaney & Rudnick 2004).

### 3.1. Outer Ejecta Detection and Spectral Discrimination

The detection of so many new outlying ejecta knots in such a relatively small area suggested that scores of undiscovered fast-moving knots of SN debris might exist elsewhere around the whole remnant. Unfortunately, the broad sensitivity of the WFPC2 F675W filter to a variety of elemental emission lines including several oxygen, nitrogen, sulfur, and argon lines precluded an easy discrimination of knot spectral properties. On the other hand, the ACS/WFC SDSS filters F625W, F775W, and F850LP could be used to distinguish outlying ejecta knots having either strong [N II] or [O II] emissions from the remnant's more commonly seen O + S bright FMK ejecta knots.

For example, as shown in Table 1, while the SDSS F625W filter, like the WFPC2 F675W filter, is sensitive to emissions from oxygen, nitrogen, and sulfur, the SDSS F775W and F850LP filters are mainly sensitive to just oxygen and sulfur emissions, respectively. Using the throughputs of the ACS/WFC + SDSS filter combinations at the wavelengths for several strong emission lines seen in Cas A ejecta, we list in Table 1 observed (uncorrected for reddening) relative fluxes for a typical S,O,Ar main shell knot ('FMK2'; Hurford & Fesen 1996) and the resulting relative fluxes that would be detected using ACS/WFC with the SDSS filters.

The ability of these three SDSS filters to distinguish different types of emission knots is shown in Table 2 where we list the relative line fluxes for five well-studied main shell ejecta knots ('FMK 1- FMK 5'; Hurford & Fesen 1996) along with three relatively bright outer ejecta knots. Spectra for these three outlying knots covering the  $6000 - 7500 \text{ \AA}$  wavelength region can be seen in the left-hand panels of Figure 2. As seen from this table, SDSS filter flux ratios for Cas A's main shell FMKs typically lie between  $\sim 0.25 - 1.0$ . The one exception is FMK 4 whose observed  $4000 - 10500 \text{ \AA}$  spectrum is dominated, not by [S III]  $\lambda\lambda 9069, 9531$  as is usually the case, but by relatively strong [O II]  $\lambda\lambda 7319, 7330$  line emission resulting in unusually high F775W/F850LP ratio and low F625W/F775W and F625W/(F775W + F850LP) ratio (also called F1/(F2 + F3); see Table 3).

In contrast to these bright main shell knots, outlying ejecta knots can show significantly different SDSS filter flux ratios. For example, Knot 15 located well above the remnant's northern limb whose  $5000 - 7500 \text{ \AA}$  spectrum shows only [N II]  $\lambda\lambda 6548, 6583$  emission ( $V_r = +4500 \text{ km s}^{-1}$ ; Fesen 2001) not surprisingly exhibits F625W/F775W and F625W/F850LP values more than an order of magnitude larger than for the five main shell ejecta knots listed. In similar fashion, the outer southeastern Knot 17, which shows an  $6000 - 7500 \text{ \AA}$  spectrum with only [O I] and [O II] line emissions (see Fig. 2), exhibits an O/S sensitive F775W/F850LP ratio nearly three times greater than even the very strong [O II]  $\lambda\lambda 7319, 7330$  emission main shell knot FMK 4. Lastly, the outer western limb Knot 19, which shows a fairly common FMK-like spectrum except for the addition of strong [N II]  $\lambda\lambda 6548, 6583$  line emission which actually dominates the  $6000 - 7500 \text{ \AA}$  region (Fig. 2), has 2-4 times higher F625W/F775W and F625W/(F775W + F850LP) ratios, half the F775W/F850LP ratio, and nearly 2-3 times the F625W/F850LP ratio of typical

main shell ejecta.

### 3.1.1. ACS/WFC Color Composite Images

*HST* ACS/WFC images covering the whole remnant using the SDSS filters were taken in March and December 2004 in order to obtain a more complete picture of both the number of outlying debris knots and the diversity of their emission properties.

A qualitative look at spectral emission variations in Cas A's high-velocity outermost ejecta can be seen in RGB color composite images using the F625W (= red), F775W (= green), and F850LP (= blue) image frames. Figure 3 shows  $20'' \times 20''$  sections of the individual ACS/WFC images covering only a portion of the eastern limb shown above in Figure 1. The three greyscale images were produced by subtracting the March from the December 2004 ACS/WFC F625W, F775W, and F850LP filter images. Also shown in Figure 3 (bottom right) is a three color composite image made from the March 2004 filter data. Ejecta knots identified through their high proper motions are indicated on each of the frames, with previously (ground-based) identified knots (Fesen 2001) marked by knot ID numbers.

From Figure 3, one sees that many knots are only visible on one or two individual filter images, leading to the strong color differences apparent in the color composite image. Similar emission variations were found for ejecta knots located in most other regions around the remnant's periphery.

Such visual inspections of the SDSS filter data set indicated not only a far larger population of high-velocity ejecta knots than previously realized, but also a much broader range of emission line properties over the 6000–10500 Å wavelength range. This, in turn, suggested a greater chemical diversity than just the notion of mostly sulfur-rich FMK-like ejecta in the main shell and jet regions and nitrogen-rich knots elsewhere. Published spectra and our new ground-based spectra of a handful of eastern limb knots support this conclusion.

However, both their faintness and the small angular separations between many individual outer knots (often less than 1''; see Fig. 3) prevented us from obtaining ground-based spectra of many individual outer ejecta knots. We have therefore used the SDSS filter images to classify ejecta knot emission properties into broad categories consistent with available knot spectra.

### 3.1.2. SDSS Filter Flux Ratios

In order to translate observed color composite differences into quantitative spectral emission differences, we measured ACS/WFC fluxes from the three SDSS filter image sets for all outer knots located along a portion of the remnant's eastern limb using the automated source extraction software package SExtractor (Bertin & Arnouts 1996). In cases where the SExtractor program failed to return a reasonable flux, or failed to return a flux at all, the knot fluxes were calculated by hand. In all cases, the fluxes were calculated using 5 pixel apertures. Background estimates were performed, by SExtractor, using a 24 pixel rectangular annulus about the isophotal limits of the object. When fluxes were calculated manually, background estimation was performed by calculating the total 5 pixel aperture flux in at least

five positions near the object (avoiding other sources) and then subtracting the mean computed "background" flux from the total object pixel sum. Most knots whose fluxes required manual computation were located near a bright background source or very close to another ejecta knot.

Flux estimates were best for the brightest, well-resolved knots (above  $5 \times 10^{-16}$  erg  $\text{cm}^{-2} \text{s}^{-1} \text{\AA}^{-1}$ ), where errors are on the 5–10% level. Moderately bright knots ( $5 - 50 \times 10^{-17}$  erg  $\text{cm}^{-2} \text{s}^{-1} \text{\AA}^{-1}$ ) suffered more from local background variations and uncertainties in knot positions, resulting in flux errors near 20–30%. Error estimates for faint knots ( $1 - 50 \times 10^{-18}$  erg  $\text{cm}^{-2} \text{s}^{-1} \text{\AA}^{-1}$ ) lie approximately at the 50% level. Fainter knots, or non-detections in one of the filters, were set to the standard deviation of the background levels of each filter as ( $\sigma_{\text{back}}$  (F625W) =  $3.9 \times 10^{-19}$  erg  $\text{cm}^{-2} \text{s}^{-1} \text{\AA}^{-1}$ ,  $\sigma_{\text{back}}$  (F775W) =  $3.7 \times 10^{-19}$  erg  $\text{cm}^{-2} \text{s}^{-1} \text{\AA}^{-1}$ ,  $\sigma_{\text{back}}$  (F850W) =  $5.7 \times 10^{-19}$  erg  $\text{cm}^{-2} \text{s}^{-1} \text{\AA}^{-1}$ ) for the purposes of determining knot type by dominant emission features.

### 3.2. The Eastern Limb

For defining the kinematic and chemical properties of the remnant's outlying ejecta, we chose to focus on the remnant's eastern limb. This area exhibits an unusually high number density of knots due to an apparent interaction of the remnant's higher-velocity ejecta with a local circumstellar cloud (Fesen, Becker, & Blair 1987). Therefore, this region might provide a more complete and unbiased assessment of the remnant's fast SN debris fragments.

The region selected lies along Cas A's eastern limb region between position angles 78.2 and 140.6 degrees covering  $\simeq 1.5$  sq arcmin in size. This avoided the NE jet to the north, which would complicate an analysis of knot emission properties with respect to radial distance, and ends near the southern edge of the faint circumstellar cloud seen in this region.

Fluxes from the F625W, F775W, and F850LP filter images were measured for a total of 229 outer emission knots identified in this east region through high proper motions measured using the March and December 2004 ACS/WFC images. The resulting F625W/F775W and F775W/F850LP flux ratios for these 229 knots are plotted in Figure 4. Also shown in this plot are the SDSS filter ratios for the five main shell knots (the purple star symbols) listed in Table 2, and the three outer ejecta knots (knots 15, 17, and 19; circled numbers) discussed above in §3.1 and also listed in Table 2.

### 3.3. Emission Classes of High-Velocity Ejecta Knots

We binned the outlying ejecta knots along the remnant's eastern limb into three emission classes, namely, [N II] strong knots, [O II] strong knots, and [S II] strong FMK-like knots. They are color-coded in Figure 4 as red, green and blue, respectively, consistent with their colored appearance on our composite images. Flux ratio criteria between these three classes were chosen to segregate knots with similar ratios seen for main shell or the outer ejecta knots with existing spectroscopy listed in Table 2.

Specifically, we chose a flux ratio for F775W/(F625W

$+ F850LP) \geq 1.0$  to separate out the [O II] strong FMKs from the [S II] strong FMKs; that is, those knots with stronger [O II]  $\lambda\lambda 7319, 7330$  emission detected via the F775W filter than the combined strength of [N II], [S III] and [S II] emissions detected in the F625W and F850LP filters. Similarly, knots with strong [N II] emissions were selected via  $F625W/(F775W + F850LP) \geq 1.0$ , thereby selecting those knots where the combined flux of [O I]  $\lambda\lambda 6300, 6364$ , [S II]  $\lambda\lambda 6716, 6731$ , and [N II]  $\lambda\lambda 6548, 6583$  emissions was greater than the sum of F775W flux, due mostly to [O II], and F850LP flux sensitive to the near-infrared [S III] and [S II] emissions. This latter ratio division is shown as a horizontal line in Figure 4. Since the observed [O I] flux rarely, if ever, exceeds the [O II]  $\lambda\lambda 7319, 7330$  flux, and the observed [S II]  $\lambda\lambda 6716, 6731$  emission is unlikely to ever exceed the combined flux of [S III]  $\lambda\lambda 9069, 9531$  and [S II]  $\lambda\lambda 10287-10370$  line emissions (Hurford & Fesen 1996; Winkler et al. 1991), then any knot for which the  $F625W/(F775W + F850LP) \geq 1.0$  requires the presence of significant [N II]  $\lambda\lambda 6548, 6583$  emission.

As shown in Figure 4, the chosen ratio criteria successfully grouped the outer FMK-like knots in with typical main shell FMKs ('FMK 1-3' and 'FMK 5'; shown as purple stars), the strong oxygen emission line ejecta like Knot 17 and FMK 4 into an [O II] bright knot class, and ejecta with dominant [N II] emission like Knots 15 and 19 into a [N II] knot category.

Measured F625W, F775W and F850LP fluxes for our selected eastern limb region placed 69 knots in the upper '[N II] knot' portion of Figure 4, 40 '[O II] knots' in the lower right-hand portion, and 120 'FMK-like knots' in the center portion of the figure. An arrow on a knot's plotted position indicates an upper or lower flux limit due to a non-detection for one or more filters (i.e., one sigma of the background flux limit, see §3.1.2). For instance, knots with arrows pointing to the left-hand portion of the plot, like some [N II] knots, have no detectable F775W ([O II]) emission above background sky variations.

A knot marked on Figure 4 with a crossbar means it was undetected in one of the filters making up its y-axis value. Since the y-axis is a combination of filter fluxes ( $y = F1/(F2 + F3)$ ) if there was no detected flux in one filter, say filter F2, one could not simply mark the knot with a directional arrow on the y-axis. However, the non-detection does lead to an uncertainty in y-axis value for that knot and the crossbar is meant to reflect that uncertainty. The length of the crossbar varies across the plot because: i) this is a log plot so a constant value has a different length along the axis, and ii) more importantly, the effect of an uncertainty of say F2 on the y-axis value depends on the specific values of F1 and F3. Crossbars were used instead of arrows because we wished to emphasize that a non-detection in a filter would not move a knot's plotted position into another knot category (below the line at  $y = 1$ ) no matter what the actual value of flux in the missing filter turned out to be.

The line of double arrowed [N II] knots appearing near the top of the [N II] section of Figure 4 represent eastern limb knots that have  $F625W/F775W$  ratios  $\geq 20$  and were undetected in both F775W and F850LP frames. These knots appear to represent highly [N II] emission dominated ejecta, even more so than the outer Knot 15 whose spectrum shows no [S II]  $\lambda\lambda 6716, 6731$  or [O II]

$\lambda\lambda 7319, 7330$  emissions (see Fig. 2). Knots near the upper part of the [N II] strong knot section of Figure 4 have  $F625W/(F775W + F850LP)$  ratios approaching 50 or more.

Below we briefly discuss three main types of high-velocity, outer emission knots found in this ACS/WFC survey.

### 3.3.1. [N II] Emission Knots

Within our selected eastern limb region, dozens of knots were found to show a F625W flux comparable or greater than the total F775W + F850LP fluxes. For these cases, the F625W flux is most probably due to strong [N II]  $\lambda\lambda 6548, 6583$  emission rather than H $\alpha$ , [S II], or [O I] emissions. This is because of the 43 strong [N II] emission outer knots with published line strengths [O I] and [S II] emissions were not detected and [N II] emission was always much stronger than H $\alpha$ , with only three exhibiting H $\alpha$  emission at readily detectable levels, i.e., [N II]  $\lambda 6583/\lambda\alpha = 3 - 4$  (Fesen 2001). Thirty of the 43 knots were bright enough to set meaningful [N II]  $\lambda 6583/\lambda\alpha$  lower limits and had typical values  $\geq 5$ , with 20% above 10.

If the observed F625W emission was due to [O I]  $\lambda\lambda 6300, 6364$  and/or [S II]  $\lambda\lambda 6716, 6731$  emission then, based on existing spectra, these knots should have been easily detected through [O II] emission in the F775W images or through strong [S II] and [S III] emission in F850LP images. This was not the case for 69 eastern limb knots indicating these knots have an optical (6000–10500 Å) spectrum with a significant contribution from, if not dominated by, [N II] emission.

Many of the brighter F625W strong emission knots match known [N II] dominant emission knots previously identified through ground-based images and spectra (e.g., Knots 4, 5, and 7). A 6000–7500 Å spectrum of an eastern limb ejecta clump not previously studied spectroscopically, labeled 'East 1', is shown in the upper right-hand panel of Figure 2 (see Table 3 for coordinates and fluxes).

A spectrum of another eastern limb knot, 'East 3', with F625W emission due in part to the presence of moderately strong [N II] emission is shown in the lower right-hand panel of Figure 2. This knot failed our strong [N II] knot flux criteria test (i.e.,  $F625W/(F775W + F850LP) \geq 1.0$ ) and was classified as an FMK-like outer knot even though, unlike any main shell FMK, it shows some appreciable [N II] emission.

### 3.3.2. [O II] Emission Knots

Both our color composite images and the plotted knot filter fluxes on the right-hand portion of Figure 4 indicated a surprising number of knots with spectra dominated by F775W flux. Strong F775W emission indicates a high probability for strong [O II]  $\lambda\lambda 7319, 7330$  line emission since the only other significant emission lines in the F775W filter's passband are the [Ar III]  $\lambda\lambda 7136, 7751$  lines. However, even for those rare knots having exceptionally strong argon emission lines (e.g., the 'calcium FMK'; Hurford & Fesen 1996), [S II] and [S III] emissions still dominate the optical spectra and thus would be plotted on Figure 4 in with the more common [S II] strong FMKs. Therefore, strong F775W emission is a good marker for unusually strong, if not dominate, [O II] line emission.

In the eastern limb region, 40 knots were identified as having a spectrum dominated by [O II] emission. Examples of these [O II] F775W bright knots can be seen in the color composite image of Figure 3 (lower right-hand panel). The group of green knots in the lower right portion of the color composite make up Knot 17A, an ejecta clump first identified from ground-based images and exhibiting spectra similar to the more southern Knot 17 (see Fig. 2; middle panels). This knot was one of a small cluster of outer ejecta knots (Knots 16, 17, 17A, and 17B) for which earlier low-dispersion spectra showed strong oxygen emission lines (Fesen 2001). Their limited spatial distribution along a section of the SE limb had initially made them appear to be simply a few odd, high-velocity ejecta clumps, not representatives of a large and well distributed subclass of outer ejecta which we now identify as strong [O II] outer knots.

### 3.3.3. FMK-like Knots

In our color composite images, FMK-like knots appear white or purple due to strong F625W and F850LP fluxes arising principally from [S II]  $\lambda\lambda 6716, 6731$  and [S III]  $\lambda\lambda 9069, 9531$  emissions. These knots typically occupy the middle of the filter flux ratio plot shown in Figure 4, as do the four bright main shell knots previously discussed and shown here as purple star symbols.

Earlier ground-based surveys had found that nearly all outlying FMK-like knots were located in either the northeast or southwest jet ejecta regions. However, the deeper and higher spatial resolution *HST* images reveal a more extensive distribution of such high-velocity FMK-like ejecta. In the eastern limb section for example, we identify 120 [S II] strong FMK-like outer knots. Virtually all of these knots are small and faint, and consequently, they fell below the detection limit of the moderately deep and broadband (FWHM = 250 Å) [S II]  $\lambda\lambda 6716, 6731$  imaging survey of the remnant (Fesen 2001).

### 3.4. Outer Knot Kinematics and Distribution

Histograms for the radial distances for all 229 identified knots in our selected eastern limb region grouped by emission type are shown in Figure 5. Radial distances for these knots, measured from the remnant's estimated center of expansion (Thorstensen et al. 2001), are in the range 135" – 195" (2.2 – 3.2 pc). As shown in this figure, [N II] bright knots tend to lie at greater distances (in projection) than the [O II] bright knots which, in turn, lie coincident with or slightly ahead of the FMK-like knots. Mean distances for the [N II], [O II], and FMK-like knots are 168", 163", and 158" (= 2.8 pc, 2.7 pc, 2.6 pc), respectively. The observed range of radial distances, when converted to average transverse velocities (assuming an age of 320 yr and a distance of 3.4 kpc) correspond to velocities of 7000 – 9500 km s<sup>-1</sup>.

For 217 of the 229 eastern limb knots we were able to estimate transverse velocities directly from proper motion measurements. Positional displacements were measured using WCS aligned January 2002 WFPC2 F675W and March 2004 ACS/WFC F625W, F775W, and F850LP images. Measured proper motions relative to observed knot radial distances are plotted in Figure 6. The line shown is a least squares fit to the radial distance vs. proper motion for all knots and has a slope of  $2.9 \pm 0.2$  mas yr<sup>-1</sup> arcsec<sup>-1</sup>. The [N II] knots exhibit the

highest proper motions, up to 0.6" yr<sup>-1</sup>, with somewhat smaller systematic values for the [O II] and FMK-like knots. Transverse velocities derived from these proper motions grouped by knot emission type yield mean expansion velocities of 8100, 7900, and 7600 km s<sup>-1</sup> for 63 N-rich, 37 O-rich, and 117 FMK-like knots, respectively.

Consistent with their greater average radial distances (Fig. 5), [N II] knots show the highest maximum transverse velocities, up to 9300 km s<sup>-1</sup>, followed by the FMK-like knots with velocities up to 9100 km s<sup>-1</sup>, and then [O II] knots of up to 9000 km s<sup>-1</sup>. These velocities significantly exceed the maximum space velocity of 6000 km s<sup>-1</sup> seen for main shell ejecta (Lawrence et al. 1995; Reed et al. 1995). However, knots in all three classes with the smallest radial distances ( $\approx 140" - 160"$ ) show a marked decrease in observed proper motions and these tend to lie at a projected positions just ahead of main shell knots. This effect is seen for all three knot emission classes and may indicate stronger deceleration by the reverse shock. Conversely, the true slope may actually be steeper than shown with the most distant knots the most decelerated.

Finally, the location of these outlying optical knots categorized by their measured filter flux ratios relative to the remnant's faint outermost X-ray emission is shown in Figure 7. Here the March 2004 red [N II], green [O II], and blue FMK optical knot positions are overlaid onto the *Chandra* 1 Ms exposure (right panel), itself color coded by isolating Si (1.8–2.0 keV), Fe K (6.5–7.0 keV), and continuum (4.2–6.3 keV) emissions following Hwang et al. (2004). The three eastern limb knots (E1–E3) discussed above for which we obtained spectra are marked in the left-hand panel which shows just the remnant's Fe X-ray emission detected by *Chandra*. One sees from this figure that nearly all the outer eastern limb knots lie near or out beyond the remnant's forward shock front. Importantly, nearly all the strong [O II] knots which we have identified via filter ratios lie (in projection) out ahead of the remnant's bright Fe-rich X-ray emitting ejecta.

## 4. DISCUSSION

A remnant's outermost debris may carry clues about both the chemistry of the progenitor's outer layers and about the dynamics of the SN explosion. Our *HST* imaging of the Cas A remnant has revealed a surprisingly large population of fast-moving ejecta outside of the NE and SW jet regions. These ejecta knots lie coincident with or out beyond the remnant's current forward shock front position (as seen in X-rays; see Fig. 1) and exhibit a wide range of filter flux ratios indicative of a significant chemical diversity, confirmed by spectral data (Figs. 2–4).

While optically emitting debris constitute only a small fraction of the total ejected mass, the remnant's fastest moving material is perhaps best studied optically. For example, the NE and SW jets can be optically traced about 80 arcsec farther out than in radio or X-rays and only a handful of outer ejecta knots around the rest of the remnant are visible in even the deepest radio or X-ray images. On the other hand, outlying ejecta knots are seen in the optical due to their interaction with surrounding ISM/CSM which generate  $\sim 100$  km s<sup>-1</sup> internal shocks driven into the knot by the high stagnation pressure behind the knot's bow shock. Consequently, what one sees

may be a biased view of the distribution of outer ejecta. Because the visibility of outlying optical knots depends upon whether they have recently encountered local ISM/CSM clouds or the forward and reverse shock fronts, combining results from different regions around the remnant might lead to a seemingly greater dispersion of chemical abundance variations with radial distance. This, plus the unlikely smooth and spherical expansion of the progenitor's outer layers, make uncertain apparent correlations of outer ejecta kinematic versus chemical properties when summed across the whole remnant. Consequently, we restricted the present study to just a relatively small, limited region along the Cas A remnant's eastern boundary where the ejecta appear to be interacting with an extended CSM cloud.

#### 4.1. Outer Knot Abundances

General spectral properties of outer emission knots were determined by the use of filter flux ratios and we have identified three main classes of outer ejecta: 1) Knots dominated by  $[\text{N II}] \lambda\lambda 6548, 6583$  emission; 2) Knots dominated by oxygen emission lines especially  $[\text{O II}] \lambda\lambda 7319, 7330$ ; and 3) Knots with emission line strengths much like those seen in the FMKs found in the main shell. The histograms shown in Figure 5 make a compelling case that, at least for the eastern limb region studied, the emission-line properties and hence likely chemical properties of Cas A's highest velocity ejecta correlate fairly well with expansion velocity.

Because few spectra are available for the nearly 230 outer knots found within our selected eastern limb region, accurate and unambiguous abundance ranges are not possible for the different knot types from the broadband filter measurements. However, the observed range of flux values, when taken together with representative knot spectra (see Fig. 2), offer qualitative estimates on relative nitrogen, oxygen, and sulfur abundances.

Using the modified Raymond (1979) shock code described in Blair et al. (2000), several models were run for shock speeds of  $50 - 100 \text{ km s}^{-1}$  assuming knot preshock densities  $\simeq 10^{2-3} \text{ cm}^{-3}$ . The log of the abundances of oxygen and nitrogen were varied from 14 to 16 ( $\text{H} = 12.00$ ) with a sulfur abundance of 14 and other elements heavier than Ne set at or below solar values. These model results indicate that while  $[\text{S III}]/[\text{O II}]$  is sensitive to shock velocity, the ratio of  $[\text{N II}]/[\text{O II}]$   $\lambda\lambda 6548, 6583/\lambda\lambda 7319, 7330$  is fairly independent of shock speed and the abundances of other elements. For N/O abundance ratios of 0.1 and 10, we found  $[\text{N II}]/[\text{O II}]$  values of  $\simeq 0.5$  and  $\simeq 100$ , respectively. Such values suggest that for strong  $[\text{N II}]$  emission outer knots, i.e., knots plotted in the uppermost portion of Figure 4 such as East 1 and Knot 15 and having spectra with  $[\text{N II}]/[\text{O II}] > 20$  (cf. Fig. 2), the N/O abundance ratio exceeds unity indicating a nitrogen overabundance at least an order of magnitude over solar.

The highest-velocity ejecta in the east limb region are clearly those with dominate  $[\text{N II}]$  emission (see Figs. 5 and 6). This fact, when taken together with the presence of N-rich circumstellar material (QSFs) and the observed lack of appreciable hydrogen emission in all but a couple of outermost ejecta (Fesen 2001) support the notion that the Cas A progenitor was probably a WN Wolf-Rayet star that exploded as a core-collapse SN Ib event

(Fesen et al. 1987, Fesen & Becker 1991, Vink 2004). Although recent estimates for the progenitor mass based on X-ray abundance analysis have difficulty explaining the lack of C-burning products such as Ne and Mg, the remnant's estimated oxygen mass of  $1-3 \text{ M}_\odot$  plus the excellent correlation between Si, S, Ar, and Ca abundances suggest a relatively high main sequence mass  $\simeq 15-25 \text{ M}_\odot$  (Woosley et al. 1993; Woosley & Weaver 1995; Willingale et al. 2002) not unlike that expected for a WR star progenitor.

For the strong  $[\text{O II}]$  emission knots, both our shock models as well as the metal-rich shock models presented in Morse et al. (2004) which assumed somewhat lower preshock densities suggest that a near solar abundance ratio for  $\text{O/S} \sim 10$  yields an observed  $[\text{O II}] \lambda\lambda 7319, 7330/[\text{S II}] \lambda\lambda 6716, 6731$  ratio of around 1 – 2 and a  $\text{F775W}/\text{F850LP}$  filter ratio of around one (after correcting for an  $A_V = 5$  mag and the ACS/WFC throughput). Because  $[\text{O II}]$  strong knots show  $\text{F775W}/\text{F850LP}$  ratios above 1.5 (and can exceed 10) and are unlikely to have strong  $[\text{S II}] \lambda\lambda 6716, 6731$  emission in light of  $\text{F625W}/(\text{F775W} + \text{F850LP})$  ratios between 0.07 – 0.5, such knots appear to possess O/S abundance ratios many times above the solar value. This qualitative assessment is consistent with spectra taken of such knots, (e.g., knot East 2 and Knot 17; see Fig. 2) for which only emission lines of oxygen are detected in the  $6000 - 7500 \text{ \AA}$  region.

#### 4.2. Asymmetric Element Mixing

Our discovery of a significant population of O-rich ejecta outside the forward shock front both here along the eastern limb region and elsewhere around the remnant (Hammell & Fesen 2006) may help in understanding the degree and asymmetry of compositional mixing of the Cas A SN debris. On the one hand, the very high-velocity Si and S rich ejecta in the NE and SW jets plus the presence of highly Fe-rich ejecta produced by explosive Si burning appearing outside the remnant's Si-rich shell along the NW and SE limbs has been taken as evidence for large scale turbulence and mixing due to a non-spherical expansion (Hughes et al. 2000; Fesen 2001; Willingale et al. 2002; Hwang & Laming 2003). This would appear consistent with some core-collapse models which show significant mixing and overturning of ejecta through Rayleigh-Taylor instabilities (Kifonidis et al. 2000, 2003), and which SN 1987A gave direct evidence for in the form of the apparent transport of freshly synthesized  $^{56}\text{Ni}$  from the core to the H-rich envelope (Arnett et al. 1989).

However, the presence of a layer of O-rich ejecta knots situated in between the apparent N-rich outer photospheric layer and the S-rich, FMK-like ejecta layer suggests that, at least for this limited eastern limb region away from the remnant's NE and SW jets, Cas A's chemical layers do not appear to have been completely mixed or disrupted all the way out to the surface. The outlying O-rich knots we see in Cas A exhibit spectral properties not unlike the O-rich ejecta seen in the LMC/SMC remnants N132D and 1E 0102.2-7219 where there is no evidence supporting mixing of O-rich ejecta with O-burning products, i.e., Si, S, Ar, and Ca rich ejecta (Blair et al. 2000). This raises questions about just how well mixed were the O-rich and S-rich layers in the Cas A SN on

both a local and global scale.

The degree and uniformity of elemental mixing in Cas A has been a long standing question (Chevalier & Kirshner 1978, 1979; Johnson & Yahil 1984; Winkler et al. 1991; Douvion et al. 1999; Hwang et al. 2000, Willingale et al. 2002). Strong O and S lines in most main shell ejecta knots indicate that substantial mixing of the O-rich and Si+S-rich layers did indeed occur. However, there is also compelling evidence that this mixing was neither microscopic nor homogeneous on large scales. Some ejecta clumps have optical spectra with nearly only oxygen emission lines visible (Chevalier & Kirshner 1979; Winkler et al. 1991), while others have very weak or nearly absent oxygen emissions but unusually strong lines of Ca, Ar, and S (Hurford & Fesen 1996). Compared to the range of  $[S\text{ II}]/[O\text{ II}]$  emission line ratios for optical knots in the main shell, there is a fairly constant  $[\text{Ar III}] \lambda 7136/[\text{S III}] \lambda 9069$  ratio suggesting Ar and S formed at about a constant ratio from oxygen burning, in sharp contrast to the observed  $[\text{O III}] \lambda 5007/[\text{S III}] \lambda 9069$  ratio which varies by as much as a factor of 100.

The observed range of ejecta spectral properties could reflect either different degrees of explosive oxygen burning (Chevalier & Kirshner 1979) or varying levels of mixing between outer O-rich material with inner layers of O-burning products (Winkler et al. 1991). Ne and Ar line emission maps made from mid-infrared observations show an anti-correlation between the presence of neon (which is most abundant in the outermost O-rich layers) and silicon-rich ejecta pointing to a mixing process that was not homogeneous on large scales (Douvion et al. 1999).

The fact that there is no correlation of main shell ejecta abundances with expansion velocity means that there had to be some inversion of the S-rich inner layers relative to the O-rich outer layers (Chevalier & Kirshner 1979). Large scale Rayleigh-Taylor instability ‘fingers’ or incomplete explosive O-burning across different regions might help explain the degree of mixing observed. In and around R-T fingers, considerable mixing would be expected leading to O-rich and S-rich ejecta regions with a lack of element vs. ejection velocity correlation like that observed.

Kifonidis et al. (2000, 2003) found for a Type Ib SN model with  $4.2 M_{\odot}$  that R-T instabilities form at the Si/O and O/He compositional interfaces. This lead to fragmentations of the Fe-rich core and considerable mixing of the inner  $2 M_{\odot}$  which ends up with an expansion velocity as high as  $3500 - 5500 \text{ km s}^{-1}$ . However, this velocity is less than that seen in Cas A and nearly pure Fe-rich material out beyond the Si-rich layers in Cas A’s NW and SE sections (Hughes et al. 2000; Willingale et al. 2002; Hwang & Laming 2003) would seem more consistent with a picture of strong but only regional overturning.

Kifonidis et al. (2003) also noted that the pattern of R-T overturning carries information about the geometry of neutrino-driven convection that seeds the R-T instabilities. If that is true, then the observed  $\sim 45^{\circ}$  angular size of the Fe-rich areas in Cas A may be indicating the rough scale of such neutrino-driven convection seeds.

On the other hand, high-velocity ( $v = 6500 - 10000 \text{ km s}^{-1}$ ) N-rich and O-rich ejecta at projected locations along the eastern limb out beyond the remnant’s fastest

moving Fe-rich X-ray emission material ( $6000 \text{ km s}^{-1}$ ) show that even though Fe-rich core fragments apparently penetrated the S + Si-rich mantle ejecta layer, they did not expand past the N or O-rich outer layers as happened in SN 1987A. Thus in Cas A, at some distance radially above the R-T finger instabilities, the He + N-rich and O-rich layering structure appears to have survived largely intact.

A nitrogen-oxygen-iron layering can be seen in Figure 7 where the majority of optical N-rich and O-rich knots lie in projection ahead of the Fe-rich ejecta detected in the X-rays. While not lying exactly in the plane of the sky, this Fe-rich material is seen to extend out to a maximum radius of  $145'' - 165''$ , in this region, corresponding to an average expansion velocity of around  $7300 - 8300 \text{ km s}^{-1}$ . De-projection of its observed radial velocity of  $-1000$  to  $-1500 \text{ km s}^{-1}$  (Willingale et al. 2002) would only move it a few arcseconds farther eastward, insufficient to extend it out beyond either the N-rich or O-rich outer ejecta knots which lie at radial distances of  $150'' - 190''$  and  $145'' - 185''$ , respectively (see Fig. 5).

Hwang & Laming (2003) and Laming & Hwang (2005) comment that any Fe-rich debris ejected farther out than seen in the *Chandra* image would have encountered the reverse shock at an earlier epoch and thus could have cooled down below the X-ray emitting temperature range. However, the coincidence of the inner edge of the O-rich ejecta we have detected with the outermost Fe-rich X-ray emitting material seen in *Chandra* Fe K image is striking (left panel, Fig. 7) suggesting that we’re seeing most of the fastest-moving Fe-rich material in this region. This holds true for the cooler Fe L emission as well which has about the same spatial distribution and extent as that of Fe K (Hwang, Holt, & Petre 2000).

However, there may be a causal relation between Fe-rich ejecta and formation of these outlying ejecta knots. As can be seen from Figure 7, the projected space density of the outer optical ejecta knots may be correlated with the outermost Fe-rich X-ray emitting ejecta. For example, the cluster of optical knots around Knot E2 lies at the easternmost tip of the detected Fe-rich X-ray emission, with the number of knots showing a noticeable decline to both the north and south. Without knot radial velocity information, one cannot test if such projected correlations are in fact spatially real, yet the coincidences seen here are intriguing.

While radially limited layer mixing may explain the abundance pattern seen along the remnant’s east limb, this process clearly did not operate in the NE and SW jet regions. Thus the global picture of the Cas A SN explosion which emerges is one of regional and radially limited overturning of mantle and core material. Added to this scenario are the seemingly opposing NE and SW jets of much higher velocity ejecta, rich in explosive O-burning products, whose nature is not well understood. This all created the fairly complex SN remnant ejecta structure exhibiting regionally diverse abundance mixing patterns we observe today.

## 5. CONCLUSIONS

We present an analysis of broadband *HST* ACS and WFPC2 images of the young Galactic supernova remnant Cassiopeia A, and concentrate specifically on a  $\simeq 1.5$  sq arcmin region located along the easternmost limb of

the remnant. This region exhibits numerous outer emission knots that are optically visible due to an apparent interaction with a local circumstellar cloud, and therefore provide a more complete and unbiased look at the remnant's fastest debris fragments. Calibrated ACS filter flux ratios along with follow-up, ground-based spectra were used to investigate some of the kinematic and chemical properties of these outermost ejecta. These data revealed the following:

1) A substantial population of outlying, high-velocity ejecta knots exists around the remnant which exhibit a broader range of chemical properties than previously recognized. Based on the outlying knots found in the east limb region, we identify three main classes of outer ejecta: a) Knots dominated by  $[\text{N II}] \lambda\lambda 6548, 6583$  emission, b) Knots dominated by oxygen emission lines especially  $[\text{O II}] \lambda\lambda 7319, 7330$ , and c) Ejecta with emission line strengths similar to the common  $[\text{S II}]$  strong FMK ejecta of the main shell. Mean transverse velocities derived from observed proper motion for 63 N-rich, 37 O-rich, and 117 FMK-like knots found in this region are 8100, 7900, and 7600  $\text{km s}^{-1}$ , respectively.

2) The discovery of a significant population of O-rich ejecta situated in between the suspected N-rich outer photospheric layer and S-rich FMK-like ejecta suggests that the Cas A progenitor's chemical layers were not completely disrupted by the supernova explosion outside of the remnant's NE and SW high velocity 'jet' regions.

3) We find that most O-rich outer ejecta along the remnant's eastern limb lie at projected locations out beyond ( $v = 6500 - 9000 \text{ km s}^{-1}$ ) the remnant's fastest moving Fe-rich X-ray emission material ( $6000 \text{ km s}^{-1}$ ) along the

eastern limb. This suggests that penetration of Fe-rich material up through the S and Si-rich mantle did generally not extend past the progenitor's N or O-rich outer layers as had been previously assumed.

The chemical and dynamical picture of Cas A that emerges is one of large, regional overturning involving both mantle and core material, separated by areas where the initial He + N-rich, O-rich, and Si + S-rich layering survived fairly intact. This generated a fairly complex remnant structure with numerous clumps of reverse shocked ejecta showing a wide diversity of chemical abundances.

Future investigations of the Cas A remnant using this *HST* image data set will include a full catalog of all optically visible outlying ejecta knots, analysis of the remnant's ejecta expansion asymmetries, and knot emission variability and ablation effects due to high speed passage through the local ISM/CSM.

We thank P. Hoeflich for helpful discussions, D. Patnaude for help with the Chandra X-ray data reduction, and J. Thorstensen for assistance with the celestial coordinate transformations. This work was supported by NASA through grants GO-8281, GO-9238, GO-9890, and GO-10286 to RAF and JM from the Space Telescope Science Institute, which is operated by the Association of Universities for Research in Astronomy. RAC is supported by NSF grant AST-0307366 and CLG is supported through UK PPARC grant PPA/G/S/2003/00040.

## REFERENCES

Arnett, D., Fryxell, B., & Mueller, E. 1989, *ApJ*, 341, L63  
 Bertin, E., & Arnouts, S. 1996, *A&AS*, 117, 393  
 Blair, W. P., Morse, J. A., Raymond, J. C., Kirshner, R. P., Hughes, J. P., Dopita, M. A., Sutherland, R. S., Long, K. S., & Winkler, P. F. 2000, *ApJ*, 537, 667  
 Chevalier, R. A., & Kirshner, R. P. 1978, *ApJ*, 219, 931  
 Chevalier, R. A., & Kirshner, R. P. 1979, *ApJ*, 233, 154  
 Delaney, T., & Rudnick, L. 2004, *Advances in Space Research*, 33, 422  
 Douvion, T., Lagage, P. O., & Cesarsky, C. J. 1999, *A&A*, 352, L111  
 Fabian, A. C., Willingale, R., Pye, J. P., Murray, S. S., & Fabbiano, G. 1980, *MNRAS*, 193, 175  
 Fesen, R. A. 2001, *ApJS*, 133, 161  
 Fesen, R. A., Morse, J. A., Chevalier, R. A., Borkowski, K. J., Gerardy, C. L., Lawrence, S. S., & van den Bergh, S. 2001, *AJ*, 122, 2644  
 Fesen, R. A., & Becker, R. H. 1991, *ApJ*, 371, 621  
 Fesen, R. A., Becker, R. H., & Blair, W. P. 1987, *ApJ*, 313, 378  
 Fesen, R. A., & Gunderson, K. S. 1996, *ApJ*, 470, 967  
 Ford, H. C., et al. 1998, *Proc. SPIE*, 3356, 234  
 García-Segura, G., Langer, N., & Mac Low, M.-M. 1996, *A&A*, 316, 133  
 Gotthelf, E. V., Koralesky, B., Rudnick, L., Jones, T. W., Hwang, U., & Petre, R. 2001, *ApJ*, 552, L39  
 Hammell, M. C., & Fesen, R. A. 2006, in preparation  
 Hughes, J. P., Rakowski, C. E., Burrows, D. N., & Slane, P. O. 2000, *ApJ*, 528, L109  
 Hurford, A. P., & Fesen, R. A. 1996, *ApJ*, 469, 246  
 Hwang, U., Holt, S. S., & Petre, R. 2000 *ApJ*, 537, L119  
 Hwang, U., & Laming, J. M. 2003, *ApJ*, 597, 362  
 Hwang, U., et al. 2004, *ApJ*, 615, L117  
 Kamper, K. & van den Bergh, S. 1976, *ApJS*, 32, 351  
 Kifonidis, K., Plewa, T., Janka, H.-T., & Müller, E. 2000, *ApJ*, 531, L123  
 Kifonidis, K., Plewa, T., Janka, H.-T., & Müller, E. 2003, *A&A*, 408, 621  
 Kirshner, R. A., & Chevalier, R. A. 1977, *ApJ*, 218, 142  
 Laming, J. M., & Hwang, U. 2003, *ApJ*, 597, 347  
 Laming, J. M., & Hwang, U. 2005, *Ap&SS*, 298, 33  
 Langer, N., & El Eid, M. F. 1986, *A&A*, 167, 265  
 Lawrence, S. S., MacAlpine, G. M., Uomoto, A., Woodgate, B. E., Brown, L. W., Oliverson, R. J., Lowenthal, J. D., & Liu, C. 1995, *AJ*, 109, 2635  
 Massey, P., & Gronwald, C. 1990, *ApJ*, 358, 344  
 Minkowski, R. 1968, in "Stars and Stellar Systems", 7, 623  
 Morse, J. A., Fesen, R. A., Chevalier, R. A., Borkowski, K. J., Gerardy, C. L., Lawrence, S. S., & van den Bergh, S. 2004, *ApJ*, 614, 727  
 Pavlovsky, C., et al. "ACS Instrument Handbook", Version 5.0, (Baltimore: STScI)  
 Peimbert, M., & van den Bergh, S. 1971, *ApJ*, 167, 223  
 Raymond, J. C. 1979, *ApJS*, 39, 1  
 Reed, J. E., Hester, J. J., Fabian, A. C., & Winkler, P. F. 1995, *ApJ*, 440, 706  
 Reynolds, E. M., & Goss, W. M. 2002, *ApJ*, 575, 871  
 Sirianni, M., et al. 2005, preprint (astro-ph/0507614)  
 Thorstensen, J. R., Fesen, R. A., & van den Bergh, S. 2001, *AJ*, 122, 297  
 van den Bergh, S. 1971, *ApJ*, 165, 457  
 van den Bergh, S., & Dodd, W. W. 1970, *ApJ*, 162, 485  
 Vink, J., Bloemen, H., Kaastra, J. S., Bleeker, J. A. M. 1998, *A&A*, 339, 201  
 Vink, J. 2004, *New Astronomy Review*, 48, 61  
 Willingale, R., Bleeker, J. A. M., van der Heyden, K. J., Kaastra, J. S., & Vink, J. 2002, *A&A*, 381, 1039  
 Willingale, R., Bleeker, J. A. M., van der Heyden, K. J., & Kaastra, J. S. 2003, *A&A*, 398, 1021

Winkler, P. F., Roberts, P. F., Kirshner, R. P. 1991, in  
“Supernovae: The Tenth Santa Cruz Summer Workshop in  
Astronomy and Astrophysics”, ed. S.E. Woosley (Springer-  
Verlag: New York), p 652

Woosley, S. E., Langer, N., & Weaver, T. A. 1993, ApJ, 411, 823  
Woosley, S. E., & Weaver, T. A. 1995, ApJ, 448, 315

TABLE 1  
HST ACS/WFC FILTER OBSERVATIONS AND DETECTED LINE EMISSIONS

Filter	Exposure times	Filter Bandpass <sup>a</sup>	Main Line Emissions in Filter Bandpass	ACS/WFC+Filter Throughput	Rel. Observed FMK Flux <sup>b</sup>	ACS/WFC+Filter FMK Flux
F625W (SDSS r)	4 × 600 s	5450–7100 Å	[O I] 6300,6364 [S II] 6716,6731 [N II] 6548,6583	0.42 0.44 0.43	39 100 0	16 44 0
F775W (SDSS i)	4 × 500 s	6850–8600 Å	[Ar III] 7136 [O II] 7319,7320 [Ar III] 7751	0.38 0.42 0.38	41 171 14	15 72 5
F850LP (SDSS z)	4 × 500 s	8500–10500 Å	[S III] 9069 [S III] 9531 [S II] 10287–10370	0.20 0.14 0.05	210 600 380	42 85 19

<sup>a</sup>Listed wavelengths represent approximate filter transmission cut-on and cut-off points.

<sup>b</sup>A Cas A FMK ejecta spectrum ('FMK 2'; Hurford & Fesen 1996). Values are relative to F([S II] 6716,6731) = 100.

TABLE 2  
OBSERVED RELATIVE FILTER FLUXES AND RATIOS FOR CAS A EJECTA KNOTS<sup>a</sup>

Rel. Line Fluxes, Filter Fluxes	FMK 1 (Shell)	FMK 2 (Shell)	FMK 3 (Shell)	FMK 4 (Shell)	FMK 5 (Shell)	Knot 19 ([N II]+FMK)	Knot 15 ([N II] Knot)	Knot 17 ([O II] Knot)
[O I] 6300,6364	55	39	29	152	157	7	≤5	22
[N II] 6548,6583	<1	<1	<1	<1	<1	130	100	≤8
[S II] 6716,6731	100	100	100	100	100	62	≤5	≤8
[O II] 7319,7320	275	171	104	1530	112	33	≤5	100
[S III] 9069,9531	689	810	440	1190	558	...	...	...
F625W (F1)	67	60	56	108	55	100	100	100
F775W (F2)	134	92	55	673	58	24	≤8	253
F850LP (F3)	135	146	78	234	103	78	≤10	30
F625W/F775W	0.50	0.65	1.00	0.16	0.95	4.17	≥12.0	0.40
F775W/F850LP	1.02	0.63	0.71	2.88	0.56	0.31	≥0.80	8.34
F625W/F850LP	0.49	0.41	0.72	0.46	0.53	1.28	≥10.0	3.30
F1/(F2 + F3)	0.25	0.25	0.42	0.11	0.34	0.98	≥5.5	0.35

<sup>a</sup>FMKs 1–5 are bright main shell ejecta clumps with published optical spectra (Hurford & Fesen 1996). Values are observed fluxes (relative to F([S II] 6716,6731) = 100 where present) multiplied by the ACS/WFC + filter throughputs (see Table 1). Knots 15, 17 and 19 are ejecta knots which lie outside the remnant's main shell of emission and have published optical spectra (Fesen 2001). Filter flux values for these knots were derived from ACS/WFC images with F(F625W) = 100.

TABLE 3  
COORDINATES AND FILTER FLUXES FOR EASTERN LIMB KNOTS 1 – 3

Knot ID	$\alpha$ (J2000) <sup>a</sup>	$\delta$ (J2000) <sup>a</sup>	F625W/F775W	F775W/F850LP	F625W/F850LP	F1/(F2 + F3)
East 1	23:23:51.01	58:49:24.9	5.76	0.63	3.62	2.22
East 2	23:23:46.85	58:48:17.4	0.28	3.18	0.88	0.21
East 3	23:23:51.05	58:49:06.2	0.98	1.12	1.10	0.52

<sup>a</sup>Positions were measured for epoch 2004.3

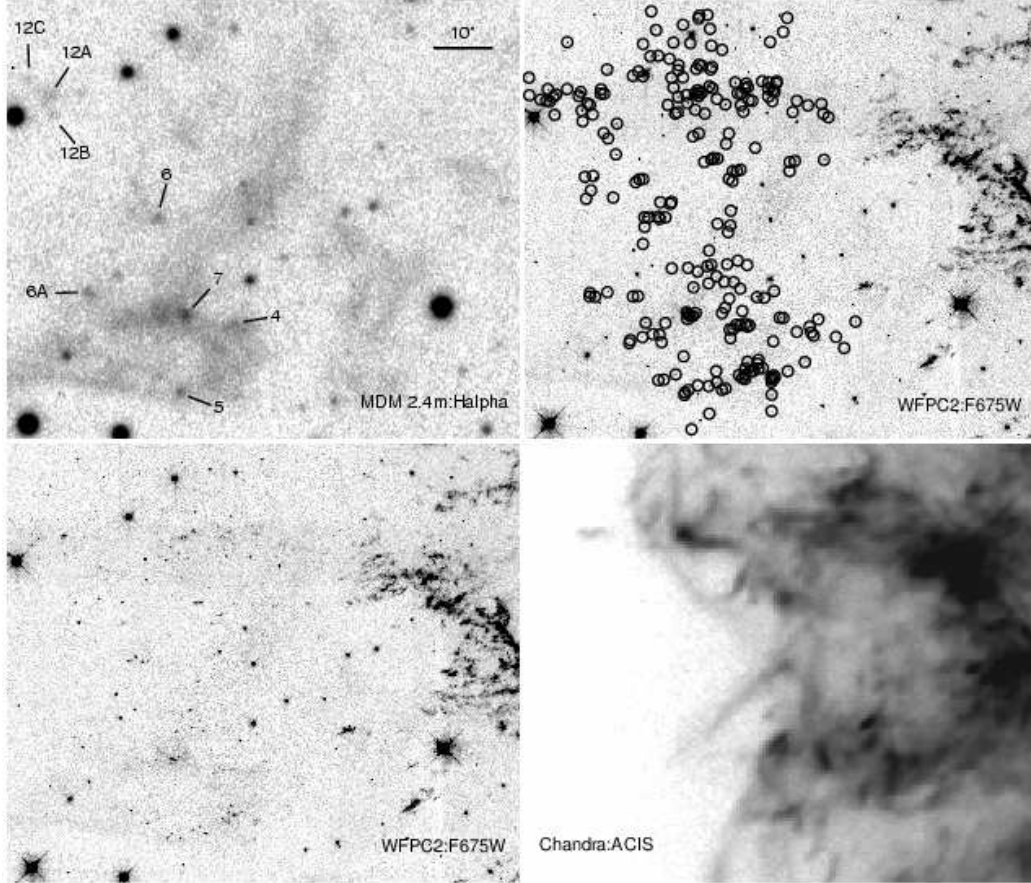


FIG. 1.— *Upper left-hand panel:* Broad H $\alpha$  (FWHM = 90 Å) ground-based image of the eastern periphery of Cas A showing the handful of previously identified outlying emission knots. *Lower left-hand panel:* January 2002 *HST* WFPC2 F675W image of the same eastern region but now revealing dozens of additional outlying ejecta knots, marked with circles in the *upper right-hand panel*. *Lower right-hand panel:* Same region showing 0.5 – 10 keV X-ray emission seen in the 1 Ms exposure *Chandra* image of Cas A.

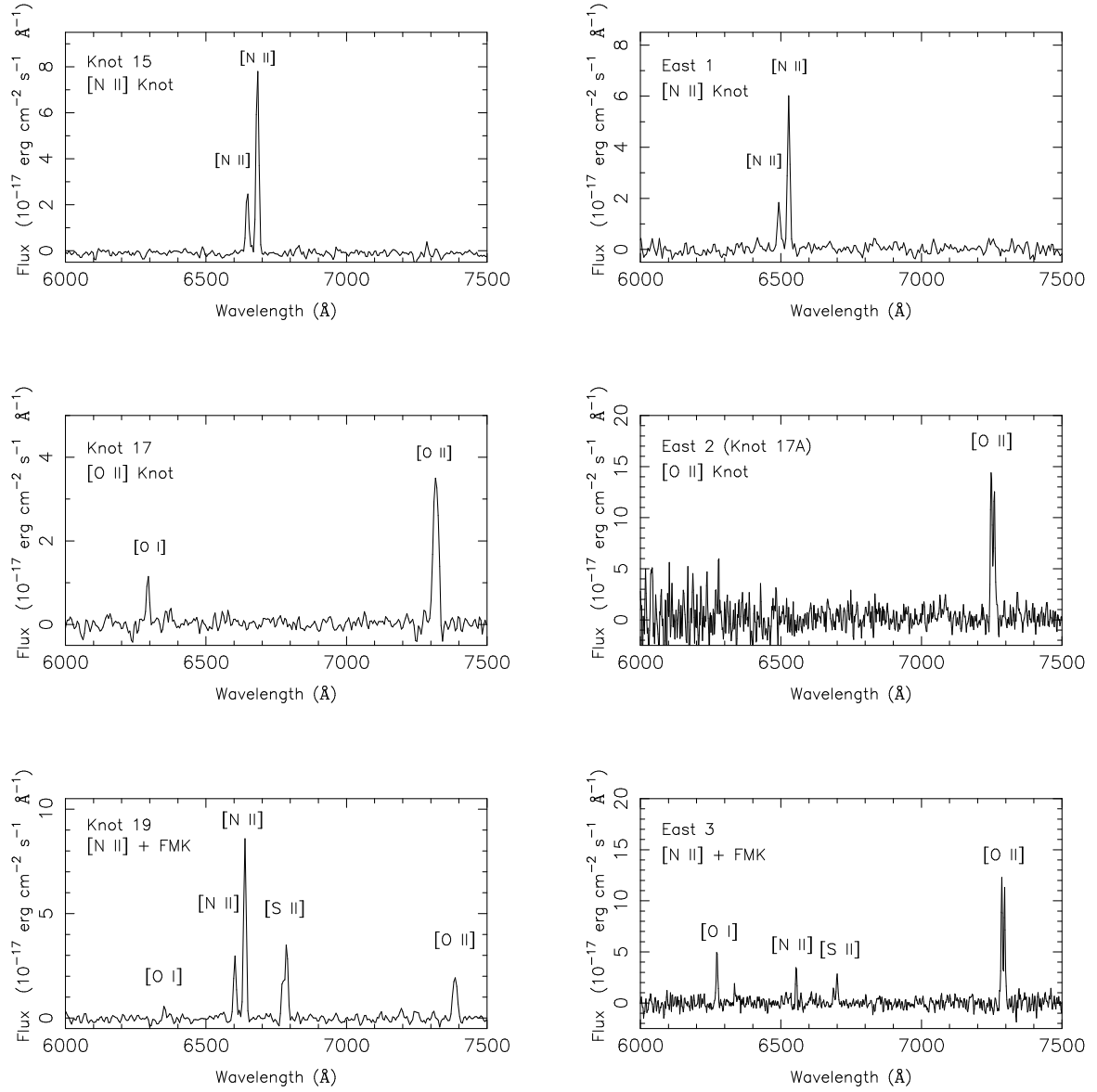


FIG. 2.— Six outer knot spectra representing the general types of outer knots emission ( $[\text{N II}]$ ,  $[\text{O II}]$ , FMK, and mixed FMKs) with left-hand panels showing examples of high S/N spectra of knots from various locations around the remnant, with the right-hand panels showing spectra of knots located only along the remnant's eastern limb.

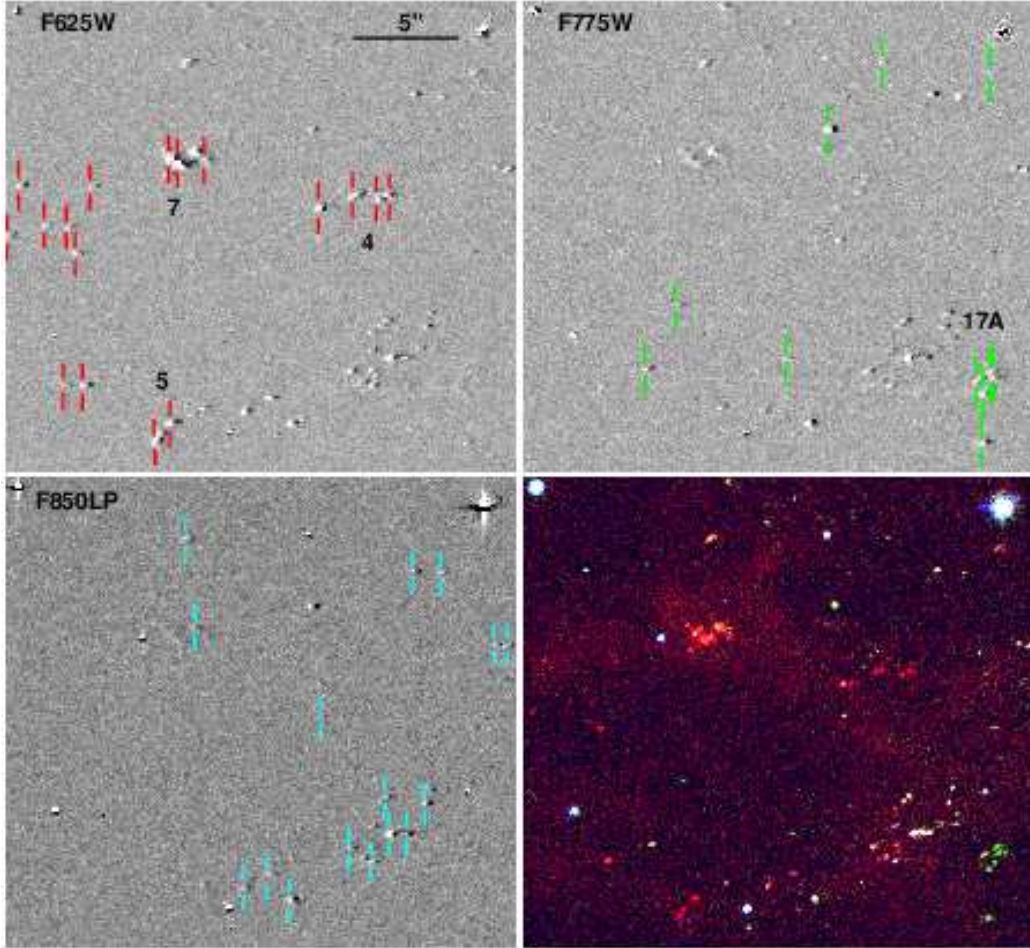


FIG. 3.— Sections of individual ACS F625W, F775W, and F850LP images are shown for a small portion of Cas A's eastern limb shown in Figure 1 around outlying ejecta knots 4, 5, and 7, along with a three color composite image (lower right-hand panel) with the images colored red, green, and blue respectively. The three greyscale images were produced by subtracting the March from the December 2004 F625W, F775W, and F850LP filter images, while the color composite was made from just the March 2004 images. Note the group of 'green' F775W strong ([O II]) knots in the lower right-hand edge of the color image.

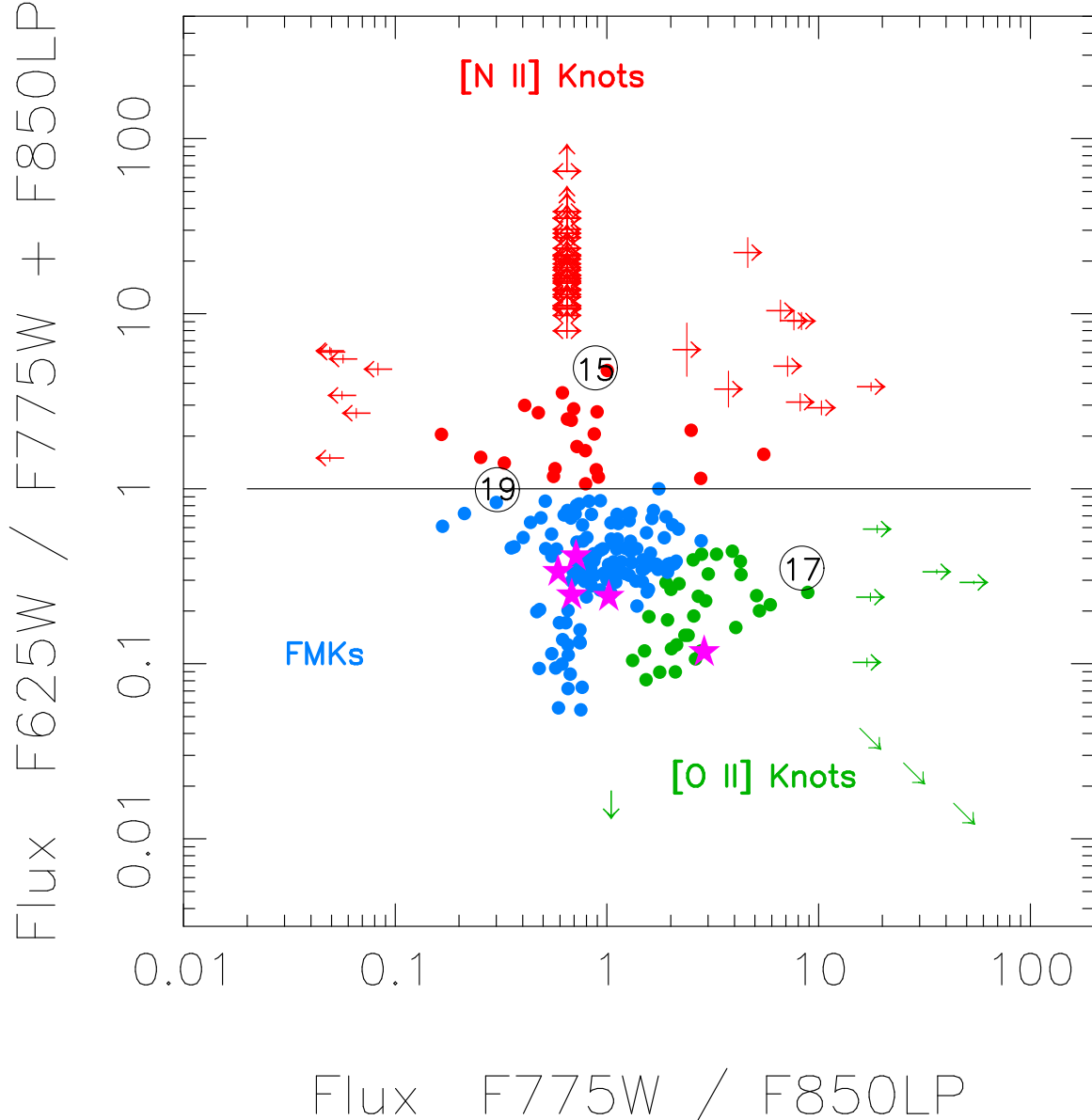


FIG. 4.— Plot of observed *HST* ACS/WFC image fluxes for the eastern outer ejecta knots for the ratios of F625W/F775W versus F775W/F850LP. Knot color coding is blue indicating FMK-like knots, red for [N II] emission strong knots, and green [O II] emission dominated knots. Arrows indicate a non-detection in at least one filter. Lines on the arrow symbols indicate how a detection equal to that of the background flux level in the non-detection filter would change the knot's plotted position. The purple star symbols represent SDSS filter ratios for the five, bright main shell knots listed in Table 2.

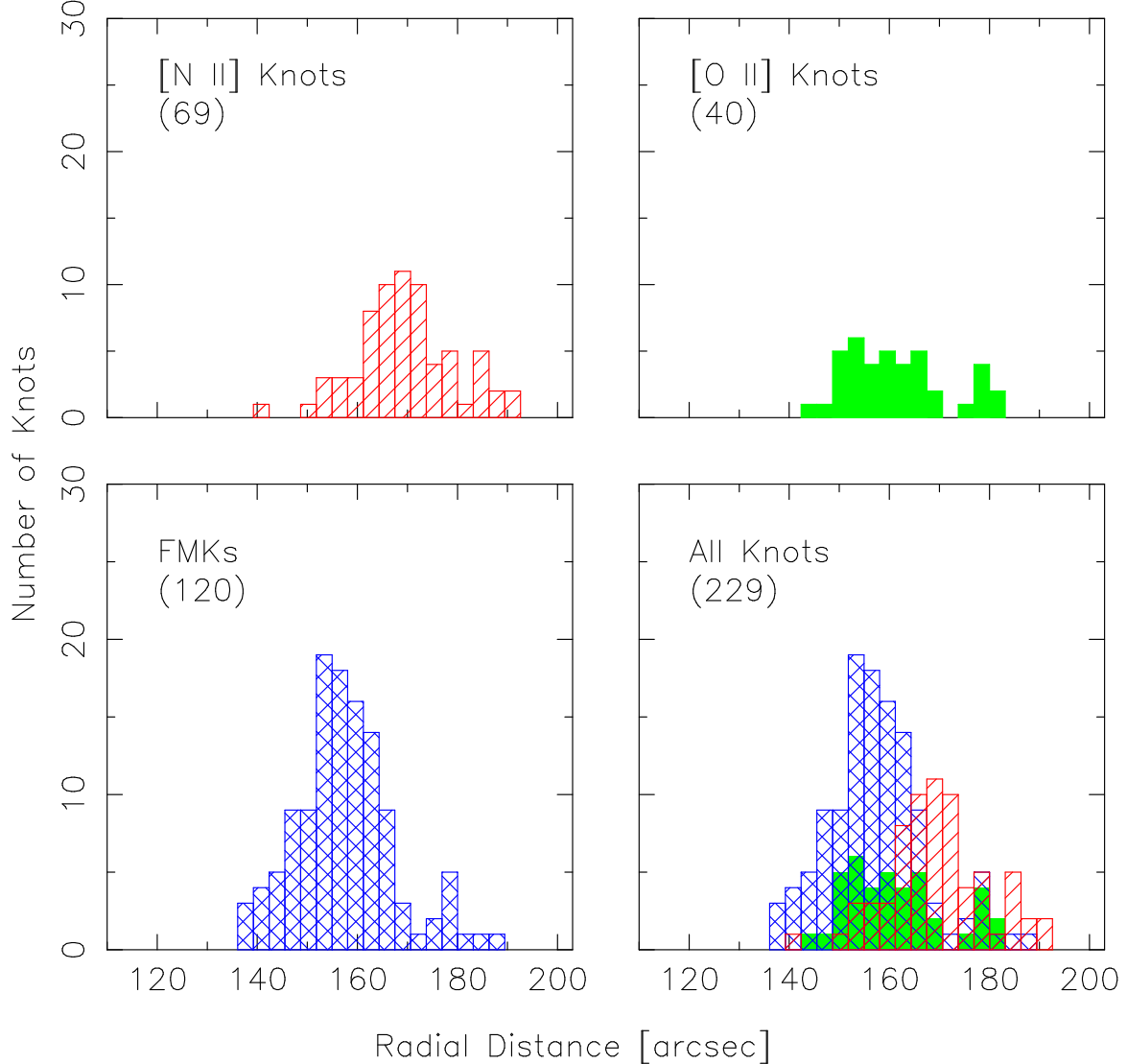


FIG. 5.— Histograms showing the radial distribution of the three types of outlying ejecta knots located in the eastern region of Cas A. Numbers in parenthesis indicate the number of knots in each category.

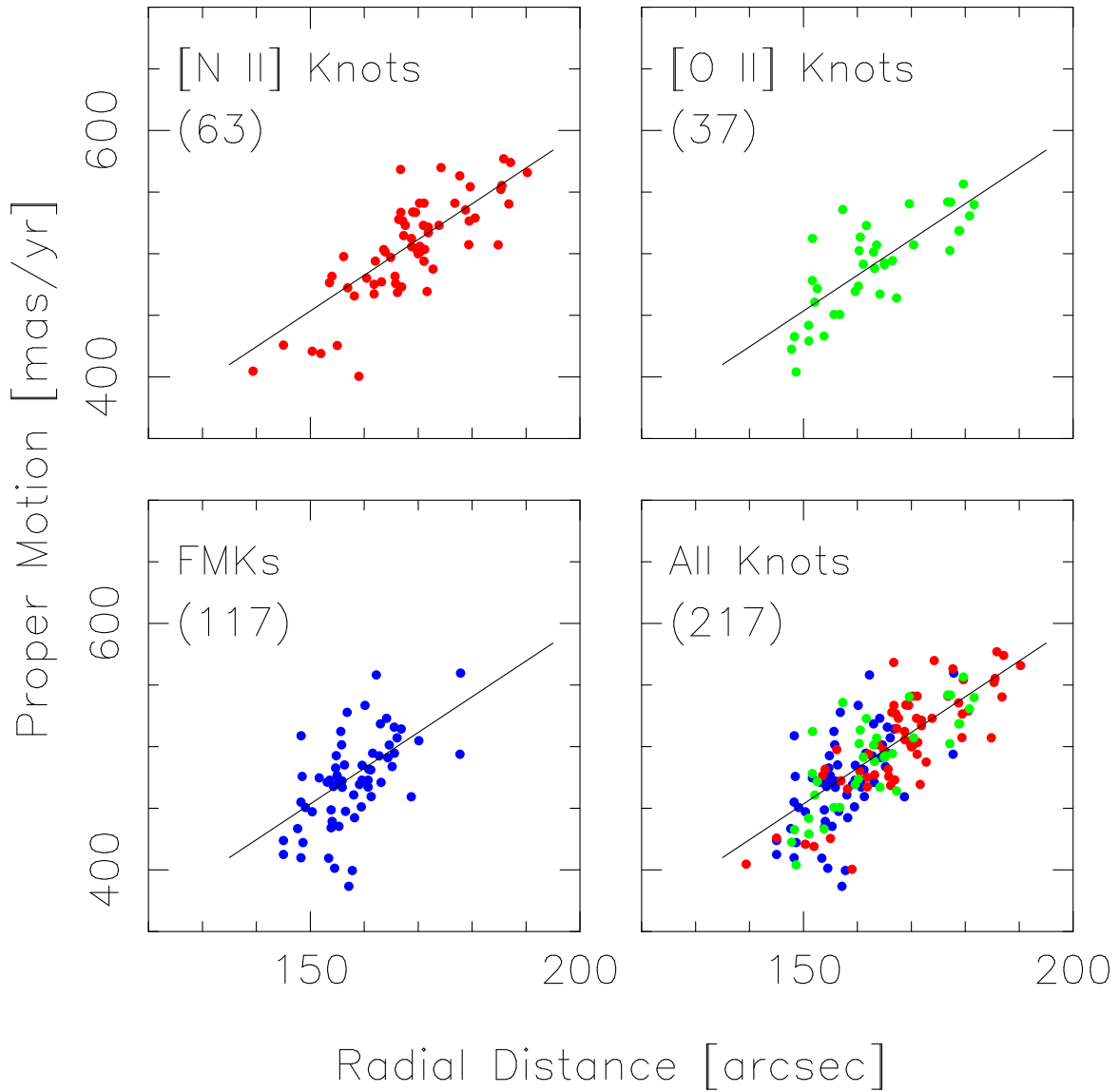


FIG. 6.— Plots showing measured 2000.0 to 2002.0 proper motions for the three types of outlying ejecta knots located in the eastern region of Cas A. Numbers in parenthesis indicate the number of knots in each category.

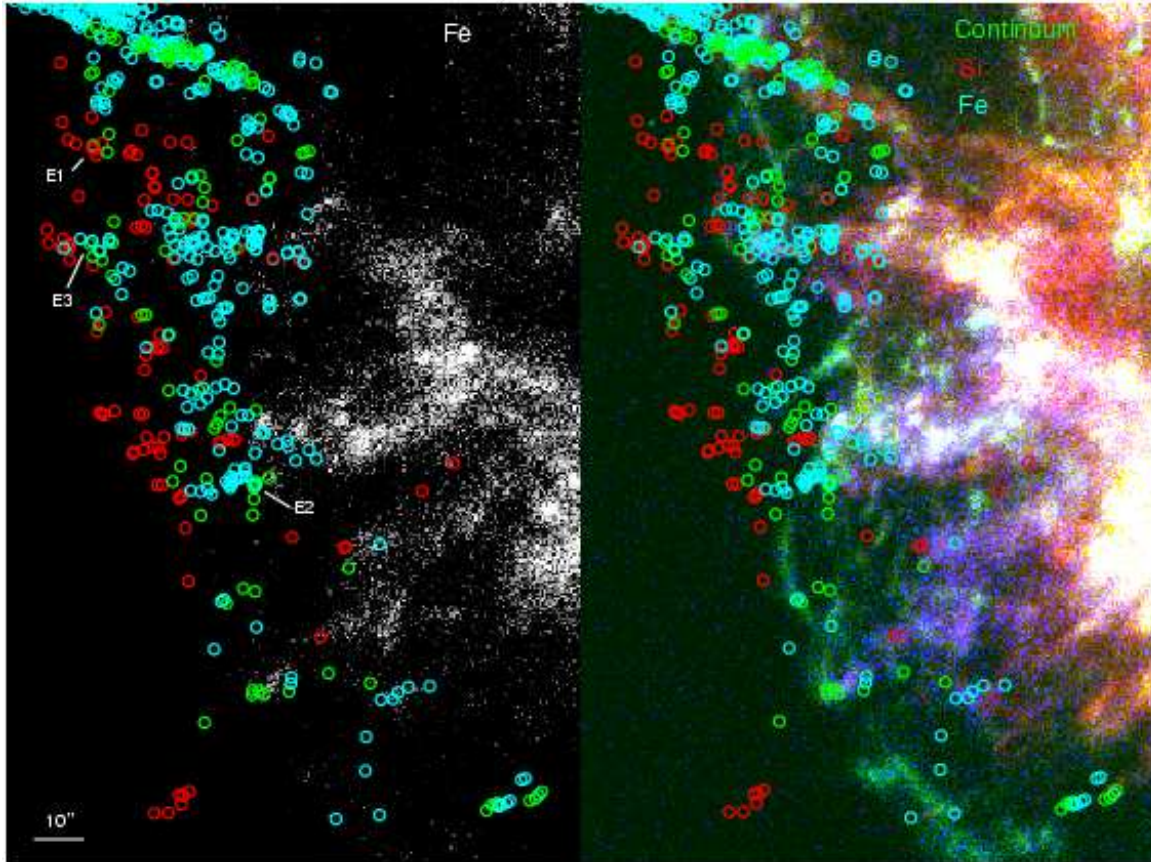


FIG. 7.— Optical outer knots positions along Cas A's eastern limb shown with respect to color coded *Chandra* 1 Ms X-ray image (red = Si He  $\alpha$  1.8–2.0 keV, blue = Fe K 6.5–7.0 keV, green = continuum 4.2–6.3 keV; right panel) and only the Fe emission (left panel). Color-coding for the optical knot symbols is the same as in Figure 4. Also marked are locations of three knots with optical spectra (Knots E1–E3; see Fig. 2).